Yanbu Journal of Engineering and Science

Volume 23 | Issue 1 Article 10

2026

Modeling and Analysis of Restoration Control in Parallel Microsource Inverters: A Case Study

Sameer Bhambri
National Institute of Technology Plot No FA7, Zone P1, GT Karnal Road, Delhi, 110036, India, sameerbhambri@nitdelhi.ac.in

Vivek Shrivastava
National Institute of Technology, Srinagar (Pauri) Garhwal, 246174, Uttrakhand, India, shvivek@nituk.ac.in

Manoj Kumawat
National Institute of Technology Plot No FA7, Zone P1, GT Karnal Road, Delhi, 110036, India, manoj@nitdelhi.ac.in

Follow this and additional works at: https://yjes.researchcommons.org/yjes

The journal in which this article appears is hosted on Digital Commons, an Elsevier platform.

Recommended Citation

Bhambri, Sameer; Shrivastava, Vivek; and Kumawat, Manoj (2026), Modeling and Analysis of Restoration Control in Parallel Microsource Inverters: A Case Study, *Yanbu Journal of Engineering and Science*: Vol. 23: Iss. 1, 154-178.
DOI: https://doi.org/10.53370/3122-3303.1216
Available at: https://yjes.researchcommons.org/yjes/vol23/iss1/10

This Research Article is brought to you for free and open access by Yanbu Journal of Engineering and Science. It has been accepted for inclusion in Yanbu Journal of Engineering and Science by an authorized editor of Yanbu Journal of Engineering and Science.

YANBU JOURNAL OF ENGINEERING AND SCIENCE 2026;23:154–178

Scan the QR to view the full-text article on the journal website

RESEARCH ARTICLE

Modeling and Analysis of Restoration Control in Parallel Microsource Inverters: A Case Study

Sameer Bhambri [a,*], **Vivek Shrivastava** [b], **Manoj Kumawat** [a]

[a] National Institute of Technology Plot No FA7, Zone P1, GT Karnal Road, Delhi, 110036, India
[b] National Institute of Technology, Srinagar (Pauri) Garhwal, 246174, Uttrakhand, India

ABSTRACT

The paper suggests a method/strategy to compensate the deviations in the system frequency and output voltage, caused by an inverter output impedance, droop coefficients terms and amplifier gain in the RDC (robust droop control) model of single phase inverter. The compensation is acquired through adopting a TDC (transient droop characteristics) enabled droop control. The suggested technique, to achieve proportionate power sharing, nominal output voltage and frequency at steady state, is applied to a communication-less system of two parallel microsource inverters. The small signal model and eigenvalue analysis are used to characterize the virtual resistor selection criteria in the inverter control block. The damping properties of power sharing responses improve when a PI controller is used in place of an integrator in a voltage-power (*V-P*) loop, The effectiveness of the suggested method is evaluated against model which is not equipped with the TDC. Subsequently, the restoration function of centralized secondary control is discussed for a standard microgrid setup, consisting of two inverters connected to bus loads via feeders. The control mechanism is illustrated to fix voltage and frequency of microgrid. The synchronous reference frame, also known as the *d-q* reference frame, describes the submodels of inverter control, such as droop controller, voltage controller, current controller, etc., in order to derive nonlinear equations that represent the dynamics of the system. The procedural steps for obtaining the small-signal model are thoroughly described. The concept of VI (virtual impedance) is discussed followed by the control algorithm to obtain its optimum parameters. The proposed schemes/models are verified through time domain simulations in Matlab/Simulink tool.

Keywords: Controller, Compensation, Droop, Error, Microgrid, Power sharing, Secondary, TDC, Virtual

1. Introduction

Power system planners have been debating the existence and development of an electrical power system for over a century. Since generation facilities, which produce electricity from sources like fossil fuels, hydro, nuclear, etc., are situated far from consumers, a typical power system structure consists of generation, transmission, and distribution facilities that distribute power to various consumers/loads. Most of the power plants connected to one another at the transmission level, where electricity moves from generating to the load, comprise the idea of a grid. Today, in addition to the conventional generators which are connected to the high voltage transmission systems, there has been a trend of electricity generation through small generating units connected to the low voltage distribution systems for technical, economic and environmental reasons. Besides the change of scale, the change in technology has been observed in the recent past following the use of distributed energy sources, storage devices, electric vehicles etc. Distributed energy sources include variable/high speed machines, direct conversion devices like solar photovoltaics etc. The control of converters

Received 17 February 2026; revised 7 April 2026; accepted 29 May 2026.
Available online 24 June 2026

* Corresponding author.
E-mail addresses: sameerbhambri@nitdelhi.ac.in (S. Bhambri), shvivek@nituk.ac.in (V. Shrivastava), manoj@nitdelhi.ac.in (M. Kumawat).

https://doi.org/10.53370/3122-3303.1216
3122-3303/© 2026 The Author(s). Yanbu Journal of Engineering and Science. This is an open access article under the CC BY 4.0 Licence (https://creativecommons.org/licenses/by/4.0/).
Published by Yanbu Industrial College, Saudi Arabia. The journal is hosted on Digital Commons, an Elsevier Platform.

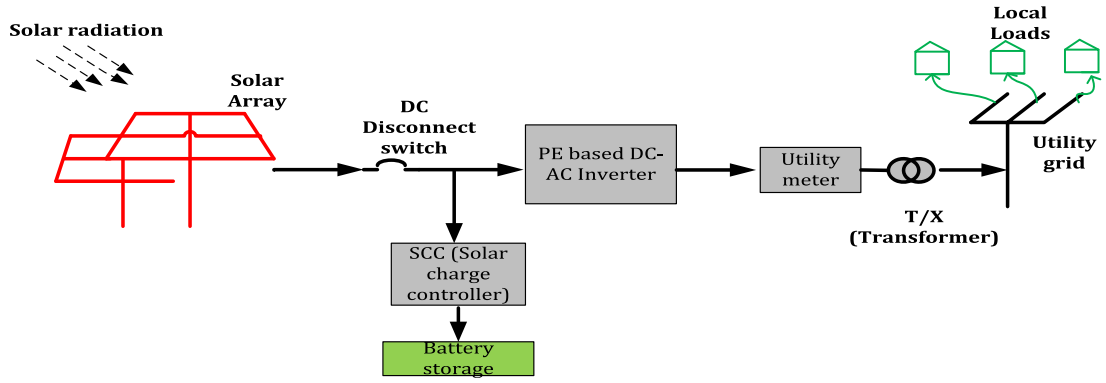

Fig. 1. Exchange of power with utility grid through solar array [3].

can not be avoided with the use of such technology [1–3]. Fig. 1 shows the schematic of a system that includes solar array, battery interfaced with solar charge controller, inverter for DC-AC conversion, utility meter, transformer, local load and grid.

Previous research has examined the mechanism of droop control for both active and reactive power regulation, as well as how it affects voltage and frequency. The droop characteristics vary depending on the type of inverter's output impedance, which is critical for enhancing the output voltage's quality. The output voltage of an inverter with resistive and inductive output impedances exhibits varying degrees of total harmonic distortion [4, 5]. Besides this, inverter output impedance also controls the load sharing accuracy of various DG (Distributed Generation) units connected in parallel [6, 7]. The microgrid, often configure as a parallel combination of multiple micro sources, has various intrinsic features, covered in primary, secondary and tertiary layers of control. The key features of multilayer control system is to regulate reactive and active power flow to provide stable voltage amplitude and frequency, besides adding reactive power compensation, harmonics current sharing and filtering in order to ensure disturbance rejection and power quality standard in microgrids. A network forming three phase isolated inverter model with its primary controls (droop control) is simulated to illustrate the operation of inverter control system [8]. In the hierarchical control of microgrid, the function of restoring voltage and frequency by secondary layer of control for two network forming converters is illustrated through a case study [9]. However, maintaining system stability in the face of fluctuating microgrid operating conditions is too a crucial design problem. The study in [10] examines the stability issues using a single-phase community microgrid concept. The power converters which are equipped with the conventional droop controllers to share active as well as reactive power, have inherent limitations of inaccurate sharing of power, circulating current etc. One such issue, encountered in low voltage dc microgrid is addressed and its solution is proposed by adaptive droop control that minimizes difference between circulating currents via virtual resistor [11]. The presence of nonlinear load in the conventional control is too a problematic situation as far as the quality of load voltage and grid current waveform is concerned [12]. The intrinsic drawbacks of the typical droop controller include erroneous power sharing to the load as a result of mismatched output impedances between inverters, noise, disturbances, numerical computations, mismatched components, etc. An UDE (uncertainity and disturbance estimator) based droop control is proposed to address these issues [13]. Various solutions are reported in the literature to address the aforesaid issues in the past. In this order, [14] presents limitations of the conventional droop control and then modified the droop control structure in the robust form thereby avoiding the condition of same per unit output impedance between parallel inverters. Inverters are also classified as L, R and C inverters based on the nature of their output impedances. The corresponding droop control equation of each type of inverter then takes different form [15]. A universal droop control is reported in [16] which can be applied for output impedance angle range lying between ($-\pi/2$ to $+\pi/2$) and takes the droop control form of resistive inverter. The same model of resistive inverter is shown to be stable in the output impedance angle range ($-\pi/2$ to $+\pi/2$) through a small signal stability tool [17]. The authors in [18] analyze the damping performance of power sharing responses through small signal analysis of resistive inverters, operating in parallel. The selection of virtual resistor and damping performance are studied by drawing bode plots of effective output impedance and eigenvalue analysis respectively. The parallel operation of inverters with different types of output impedance is made possible by universal droop controllers; however, droop controllers still have to tradeoff between power sharing and load voltage and

frequency regulation. This trade-off can be somewhat eliminated by the approach suggested in [19]. After then, the question is raised: Is accurate power sharing feasible without any deviations in output voltage and/or frequency?

Maintaining voltage and frequency within prescribed limits in an islanded operation has been remain a challenging task and widely addressed in the past. The VAr (Volt Ampere reactive) sharing among DG sources in an islanded MG is improved by proposing a self-tuning V_{nom} (Nominal Voltage) based Q-V droop control. This is accomplished by combining the system frequency and the nominal voltage computation, which drives the V_{ref} (Reference Voltage) of all DGs in a way that enhances reactive power sharing across the network. Using adaptive nominal voltage instead of fixed nominal voltage results in a noticeable improvement in VAr sharing. The suggested approach does not require feeder impedance information or rely on data sharing between sources [20]. In most of the instances, communication is employed with droop control to improve reactive power sharing issue. The technique of VI (Virtual Impedance) optimization can be applied where communication is not established in advance. An advanced optimization technique, aiming to solve two issues, is proposed in order to accommodate the system's DG units with varying capacities, the VAr estimating technique used in objective function is modified first. Secondly, to simplify the network, before optimising it to deal with a system with more number of nodes. With these enhancements, the range of applying VI optimisation method is significantly expanded [21]. An accurate VAr sharing scheme based on the optimal tuning of the complex VI for each inverter is proposed, taking into account the mismatched feeder impedances in islanded AC MGs [22]. The strategy has multiple benefits, the first being, it explicitly establishes a relationship between the assigned values for the proposed complex VI to each inverter and the mismatched values of the actual RL feeders. Secondly, there is no need of prior knowledge of feeders. In the modified voltage restoration mechanism, the proposed Q-V droop control method that reduces the effect of line impedance is proposed in [23].

A communication-free adaptive VI based droop control approach is suggested as a solution to the VAr sharing issue brought on by line impedance differences [24]. To achieve a compromise between the precision of VAr sharing and voltage drop, the adaptive VI controller is fed the VAr output and voltage of each DG. Small signal analysis is conducted to get optimal controller parameters. Communication links are used to adjust the voltage droop slope in order to correct for the mismatched voltage drops across feeders, rather than directly managing the inverter's output voltage. Even with the final adjusted droop coefficient, the controller is still able to give outstanding performance the one with the fixed droop parameters in the event of failure of communication. Furthermore, the microgrid bus voltage is shown to be barely impacted by the net control of the adaptive droop terms [25]. The concerns in sharing reactive power with precision in case of networked microgrid is revealed, therefore design of VI controller is proposed based on estimation method for network VAr sharing error [26]. GA (Genetic algorithm) is used to optimize parameters of VI of each distributed generating unit to further minimize global error of microgrid.

The performance of microgrids are also analyzed from the viewpoint of small signal stability model. A small signal based state space model of an IBMG (inverter based microgrid), including network, load and droop control is proposed and feasible ranges for inverter parameters that influence the dynamic stability, are identified [27]. Similarly a d-q reference based two bus microgrid model is established and small signal stability/participation factor based analysis is done, however solution to reactive power sharing error was not addressed [28]. In [29], the small signal stability is studied for two/three bus microgrid model with the inclusion of virtual impedance and PLL in the inverter control. A population based optimization algorithm is applied to maximize the stability index and minimize reactive power sharing error between buses. Inclusion of virtual synchronous generator model and impact of its parameters on the stability of microgrid is studied in [30] with detailed analysis. The sensitivity analysis of the modes assists in identifying their sources and fixing the feedback of signals to improve the stability [31].

The literature is already loaden with droop control of inverters, particularly the primary and secondary controls, However, the comprehensive mechanism to compensate the deviations in voltage/frequency variables due to droop terms and the output impedance in robust droop control model of $1–\varphi$ inverters is not addressed. The related work, reported in [19], addressed this issue and achieved the objective partially. The universal droop control, proposed in [16], highlighted the output impedance angle range ($-\pi/2$ to $+\pi/2$) of inverter, but deviations in voltage and frequency variables are not addressed. In [9], the secondary layer of MG control is used to address this issue. Keeping the above points in mind, the transient droop enabled inverter is proposed to compensate the deviations in full-fledged way through droop control layer only thereby proving novelty over the existing work. Secondly, one of the secondary control functions of microgrid *i.e* to restore voltage and

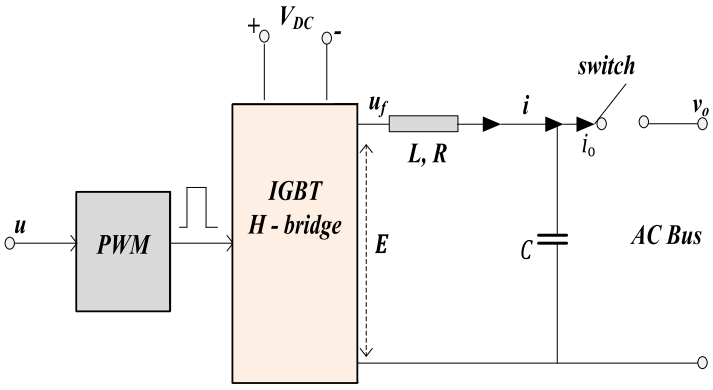

Fig. 2. 1-Φ H-bridge inverter.

frequency, is illustrated and utility of virtual impedance is cited.The objectives achieved in the paper are as follows.

1. To restore the voltage and frequency variables by adopting TDC enabled 1–Φ RDC (robust droop controller).
2. To discuss the concepts of centralized secondary control and VI in a microgrid operation.

The organization of paper is as follows. Section 2 introduces the CDC and RDC schemes followed by the proposed method to compensate deviations in the output voltage and system frequency. The Subsection 2.6 describes the small signal model associated with VSI control followed by the eigenvalue analysis to figure out the virtual resistor value. Subsequently, in the Subsection 2.7, the concept of centralized secondary control in microgrid operation is discussed followed by the detailed small signal model of microgrid in synchronous reference (*d-q*) frame. Thereafter, role of virtual impedance and associated control algorithm is also discussed. The Section 3 verifies the models/schemes described in the paper followed by the conclusion and future work.

2. Materials and methods

The models/schemes of TDC enabled inverter, small signal analysis are discussed in Subsection 2.1 and 2.6 respectively. Thereafter, in Subsection 2.7, the concept of centralized secondary control is presented fol-lowed by the small signal model of MG (microgrid) control system, under consideration.

The next subsection introduces conventional droop control associated with H- bridge in-verter and its limitations. Thereafter, need of robust droop function is described.

2.1. CDC (Conventional droop controller)

The schematic diagram of single phase H-bridge inverter is shown in Fig. 2. The description of pertinent variables and parameters is as follows. v_o is the voltage across load terminals; current i and i_o flow through the filter inductor (L) and load respectively. Filter capacitor (C) is connected across the load terminals. The pulse width modulation scheme produces signals for four switches of bridge inverter [14]. The details of control circuitry is described in the Subsection 2.5.

The voltage-active power (E-P) and frequency-reactive power (ω-Q) droop control equations for the inverter having resistive output impedance are given by 1 and 2 [4, 5]. The corresponding droop characteristics is shown in Fig. 3(i).

$$E = E^* - nP \tag{1}$$

$$\omega = \omega^* + mQ \tag{2}$$

m- frequency-reactive power droop coefficient in rad/VAr, n - voltage-active power droop coefficient in volts/watt E^*- nominal system voltage in volts, ω^*- nominal system frequency in rad/sec.

According to (1) and (2), in the steady state, the deviations in the system frequency and output voltage magnitude, are due to the terms mQ and $-nP$ respectively. These deviations become zero only when active and

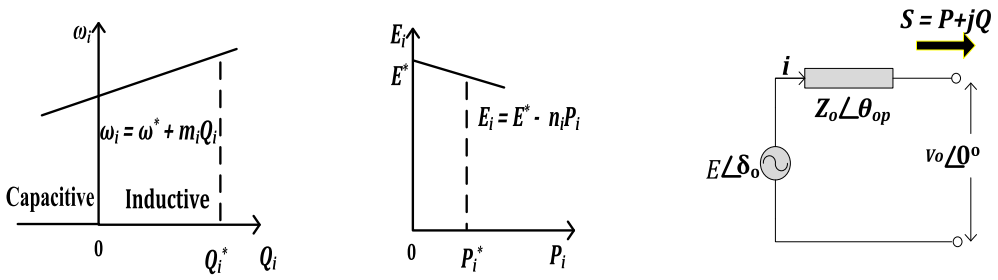

Fig. 3. (i) Droop characteristics for conventional resistive type Inverter [14] (ii) Inverter model.

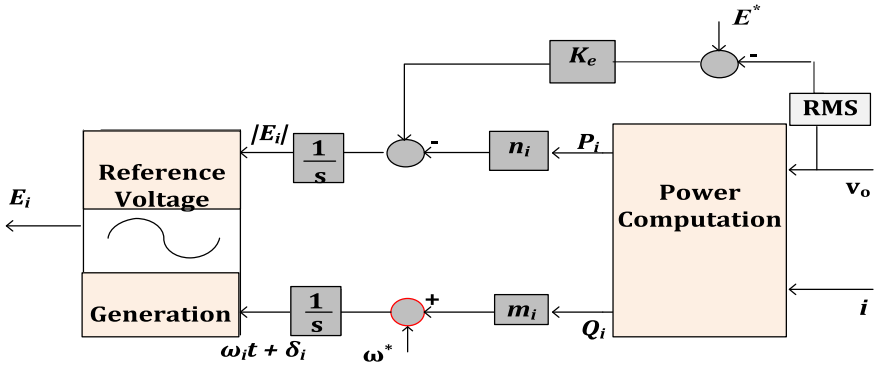

Fig. 4. RDC structure for inverter.

reactive power goes zero. The drop in the output voltage also occurs due to the output impedance (Z_o) of an inverter.

The inverter model is shown in Fig. 3(ii), Where E (volt) and δ_o (radians) are magnitude and phase angle of the reference voltage; $Z_o(\Omega)$ and θ_{op} (radians) are magnitude and angle of inverter output impedance; S, P and Q are apparent, active and reactive power; V_o (volt) is voltage of output terminals and i (amp) is current flowing through Z_o. For resistive inverter, the output impedance angle is assumed zero ($\theta_{op} \approx 0$). Under this condition, $P \sim E$ & $Q \sim -\delta_o$.

2.2. Robust droop controller

The concept ofrobust droop controller was introduced to overcome the limitations of conventional droop control. In CDC scheme, the various units connected in parallel should have same per unit output impedance in order to achieve proportional power sharing. Apart from this, the scheme also suffers with the limitation of noise, disturbances, component mismatches etc. The E-P droop characteristics, expressed in (1) is modified to (3) for RDC (robust droop control) scheme as shown in Fig. 4. However, ω-Q droop characteristics remains unchanged from (2) for RDC [6, 14, 16].

$$\dot{E} = (E^* - V_o)K_e - nP \tag{3}$$

In (3), K_e is an amplifier term (constant value); $\dot{E}$ ($\frac{dE}{dt}$) is the time derivative term of the reference voltage E. At the steady state, $\dot{E} = 0$, therefore, Eq. (3) is expressed in (4) as follows.

$$(E^* - V_o)K_e = nP \tag{4}$$

According to (2) and (3), the deviations in the output voltage and system frequency at the steady state is given by mQ and $-\frac{nP}{K_e}$ terms. However, these deviations can be controlled by adjusting m, n and K_e but their neutralization is not possible until P and Q are zero. However, this tradeoff can be eliminated to some extent with the control structure proposed in [19] as shown in Fig. 5(i).

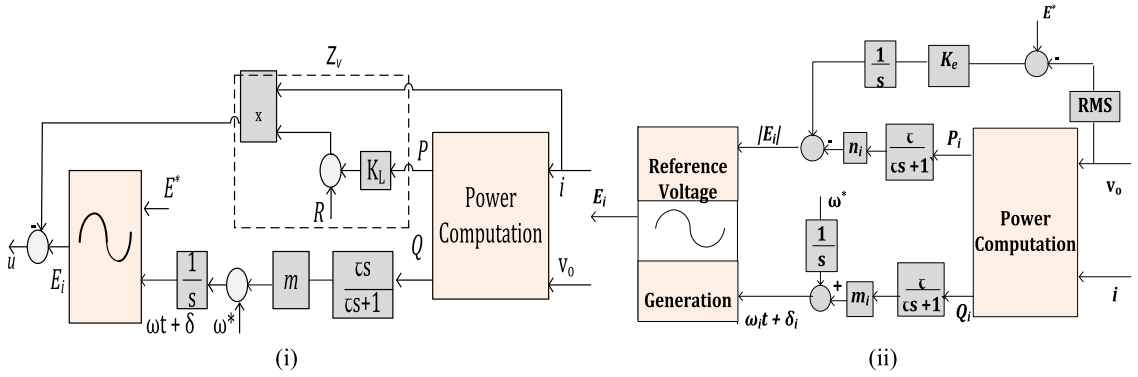

Fig. 5. (i) TDC enabled inverter [19] (ii) RDC scheme adopting the TDC method.

The following set of equations are expressed by referring Fig. 5(i).

$$E = E^* \tag{5}$$

$$\omega - \omega^* = m\widetilde{Q} \tag{6}$$

Where, $\widetilde{Q} = \frac{\tau s}{\tau s + 1} Q$

The transient droop action has a time constant (τ) term. Eqs. (7) and (8) are expressed by referring Figs. 2 and 5(i).

$$v_o = E - iZ_O \tag{7}$$

Where,

$$Z_o = sL + Z_v = sL + R + K_L P \tag{8}$$

$Z_v = (R + K_L P)$ is an adaptive virtual impedance. The output impedance (Z_o) in [19] is defined at the terminals of the load voltage and load current. It can also be defined at the terminals of the load voltage and inductor current without making much difference. The reactive power can be shared in proportion to the inverter rating at the steady state with zero frequency deviation as $\widetilde{Q}$ tends to zero. This observation can be made by referring Eq. (6). But still there are two issues unresolved. Firstly, there is deviation in the magnitude of the inverter output voltage due to drop on its output impedance and secondly, active power is not shared in proportion to inverter rating.

For resistive inverter, $sL < < R$,

$$P = \left(\frac{E - V_o}{Z_o}\right) V_o \simeq \frac{E^* - V_o}{R + K_L P} V_o \tag{9}$$

$$K_L P^2 + PR + (V_o - E^*)V_o = 0 \tag{10}$$

At the steady state, $(V_o - E^*)\, V_o$ is constant. For an equal active power (P) sharing, K_L and R should have same values for all the inverters. This can be achieved by the controller easily but proportional power sharing is still an issue.

2.3. Suggested control method

To resolve issues discussed in the previous subsection, the transient droop characteristics is incorporated in the scheme of robust droop controller as shown in Fig. 5(ii) [13]. Eqs. (11) and (12) are described for voltage-active power and frequency-reactive power loop.

$$\dot{E} = (E^* - V_o)K_e - n\widetilde{P} \tag{11}$$

$$\omega = \omega^* + m\widetilde{Q} \tag{12}$$

At the steady state, $\dot{E}$ tends to zero. Therefore,

$$(E^* - V_o)K_e = n\widetilde{P}, \tag{13}$$

Where,

$$\widetilde{P} = \frac{\tau s}{\tau s + 1}P \tag{14}$$

$$\widetilde{Q} = \frac{\tau s}{\tau s + 1}Q \tag{15}$$

Also, the steady state values of $\widetilde{P}$ and $\widetilde{Q}$ are zero as they are transient terms. Therefore, under such condition, the system frequency and output voltage settle at their nominal values as expressed in (16) and (17).

$$V_o = E^* \tag{16}$$

$$\text{and} \quad \omega = \omega^* \tag{17}$$

Eqs. (16) and (17) ensure zero deviation of the output voltage and frequency at the steady state. It proves that voltage drop due to the output impedance is compensated well. The Eqs. (14) and (15) are expressed as follows.

$$P = \left(1 + \frac{1}{\tau s}\right)\widetilde{\mathrm{P}} \tag{18}$$

$$\text{and} \quad \mathrm{Q} = \left(1 + \frac{1}{\tau s}\right)\widetilde{\mathrm{Q}} \tag{19}$$

$$P = \frac{1}{\tau}\int_0^\infty \widetilde{\mathrm{P}}dt + \widetilde{\mathrm{P}} \tag{20}$$

$$Q = \frac{1}{\tau}\int_0^\infty \widetilde{\mathrm{Q}}dt + \widetilde{\mathrm{Q}} \tag{21}$$

On letting H(s) $= \frac{\tau s}{\tau s + 1}$,

Referring Eqs. (20) and (21), it is clear that active power (P) and reactive power (Q) are shared in proportion to VA ratings of inverters as long as transient powers $\widetilde{\mathrm{P}}$ and $\widetilde{\mathrm{Q}}$ are shared in proportion. This can be achieved through the proper selection of n and m. In order to avoid the pole zero cancellation caused by H(s) and integrator blocks, the integrator positions are changed in Fig. 5(ii).

2.4. Modification in the suggested structure

The proposed structure of Fig. 5(ii) is further portrayed by placing a differentiator after the power computing block, as shown in Fig. 6. Further, the model is extended by replacing integral controller with the PI controller in E-P loop as shown in Fig. 7. The responses including active, reactive power, system frequency, output RMS voltage are shown and compared for the modified structure in the result Section 3.

2.5. Control scheme

The single phase H - bridge IGBT (insulated gate bipolar transistor) inverter circuit along with its control circuitry is under consideration for designing the resistive output impedance. The inverter is connected to an AC bus through a switch where load is assumed to be connected. The current i through filter inductor can be passed through virtual resistor block so that resistive nature of output impedance dominates. This is accomplished through a closed loop system as shown in Fig. 8.

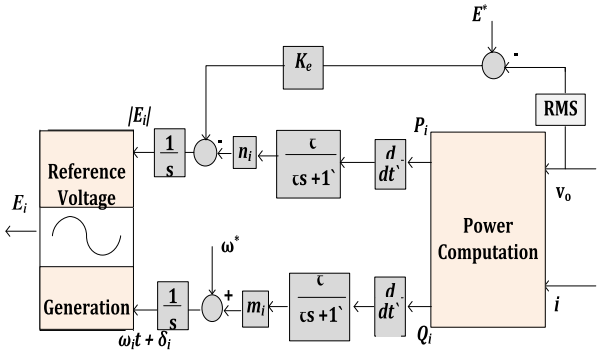

Fig. 6. RDC scheme with modified structure.

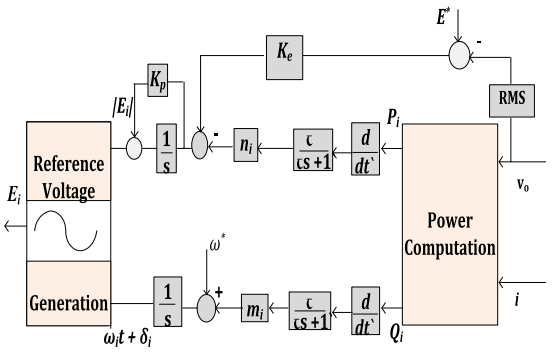

Fig. 7. RDC scheme with modified structure and PI control.

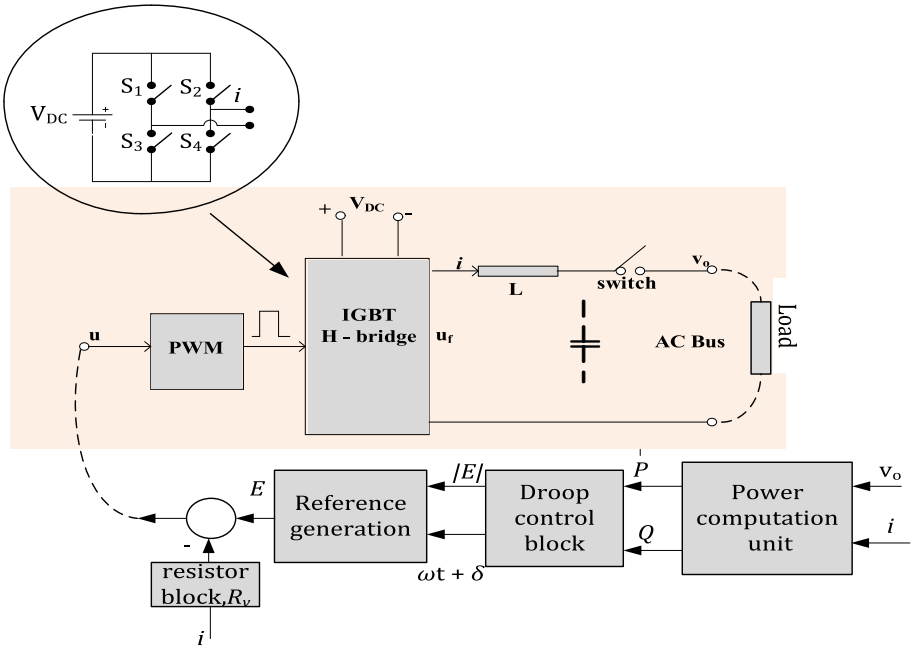

Fig. 8. Control scheme of resistive type inverter.

2.6. Small signal stability model

The objective of discussion, under this subsection, is to understand the damping characteristics of power sharing responses as well as selection of virtual resistor in the control block of an individual VSI.

The small signal stability is conducted for one inverter control block that is participating in parallel operation. Small disturbance around phase angle (δ_o), reactive power (Q) and inverter RMS voltage (E) is considered in linearizing (22) and (23).

$$P = \left(\frac{E\boldsymbol{V_o}}{\boldsymbol{Z_o}}\cos(\delta_o) - \frac{\boldsymbol{V_o^2}}{\boldsymbol{Z_o}}\right)\cos(\theta_{op}) + \frac{E\boldsymbol{V_o}}{\boldsymbol{Z_o}}\sin(\delta_o)\,\sin(\theta_{op}) \tag{22}$$

$$Q = \left(\frac{E\boldsymbol{V_o}}{\boldsymbol{Z_o}}\cos(\delta_o) - \frac{\boldsymbol{V_o^2}}{\boldsymbol{Z_o}}\right)\sin(\theta_{op}) - \frac{E\boldsymbol{V_o}}{\boldsymbol{Z_o}}\sin(\delta_o)\,\cos(\theta_{op}) \tag{23}$$

θ_{op} is inverter output impedance angle. If a small perturbation occurs around the operating point, then perturbed state vector can be written as

$$\Delta X_o^{CON} = [\Delta E\ \Delta\delta_o\ \Delta Q]^T \tag{24}$$

With the consideration of low pass filters, the power sharing equations are linearized to obtain (25) and (26).

$$\Delta P = \left(\frac{\omega_f}{s+\omega_f}\right)(\Delta E K_{PE} + \Delta\delta_o K_{P\delta}) \tag{25}$$

$$\Delta Q = \left(\frac{\omega_f}{s+\omega_f}\right)(\Delta E K_{QE} + \Delta\delta_o K_{Q\delta}) \tag{26}$$

Where, ω_f : cutoff frequency of low pass filter; 's' : Laplace operator.
The linearized form of reactive power-frequency droop equation is expressed in (27).

$$\Delta\omega = m\Delta Q \tag{27}$$

The perturbed power angle ($\Delta\delta$) and angular frequency ($\Delta\omega$) are related and expressed in (28).

$$\frac{\partial\Delta\delta_0}{\partial t} = \Delta\omega \implies \Delta\delta_0 = \frac{1}{s}\Delta\omega \tag{28}$$

Where, $K_{PE} = \frac{V_o}{R}\cos\delta_o, K_{P\delta} = -\frac{EV_o}{R}\sin\delta_o,$

$K_{QE} = -\frac{V_o}{R}\sin\delta_o, K_{Q\delta} = -\frac{EV_o}{R}\cos\delta_o$

ω_f is the cut-off frequency of low pass filter. The load, connected across output terminals is assumed resistive having value R. Therefore, small signal model of the conventional controller is obtained in the form of state space representation as shown below.

$$s\Delta X_o^{CON} = A^{CON}\Delta X_o^{CON} \tag{29}$$

The state space matrix for conventional droop control, A_{CON} is formed as

$$A^{CON} = \begin{bmatrix} -\omega_f - n\omega_f K_{PE} & -n\omega_f K_{P\delta} & 0 \\ 0 & 0 & m \\ \omega_f K_{QE} & \omega_f K_{Q\delta} & -\omega_f \end{bmatrix} \tag{30}$$

2.6.1. Small signal model of VSI control with modified structure and PI control

The perturbed state vector for the structure (in Fig. 7) is defined as-

$$\Delta X_o^{PRO} = [\Delta E\ \Delta\delta_o\ \Delta P\ \Delta Q]^T \tag{31}$$

With PI controller, the reference voltage E_o is expressed as

$$E = K_I\int\left(K_e\ (E^* - V_o) - P_i n_i\right)dt + K_P(K_e(E^* - V_o) - P_i n_i) \tag{32}$$

Subscript i ($i = 1,2$) refers to number of VSIs participating in the parallel operation.
If deviation in voltage V_0 is neglected, the Eq. (32) can be linearized to get (33).

$$\Delta E = -\left(\frac{K_I}{s} + K_p\right)n\Delta P \tag{33}$$

Now the state space representation of the proposed model is stated in (34).

$$s\Delta X_o^{PRO} = A_{PRO}\Delta X_o^{PRO} \tag{34}$$

Table 1. System parameters [14].

component	value	unit
V_{DC}	42	Volt
L (filter)	2.35	mH
C (filter)	22	μF
r (parasitic)	0.1	Ω
R_{vi} (virtual), $i = 1,2$	2, 4	Ω
E^*	12	Volt
m_i	0.1, 0.2	rad/VAr
n_i	0.4, 0.8	Volt/Watt
K_e	10	
τ	1	sec

Table 2. Steady state performance.

Variable	With compensation	without compensation
$\frac{E^* - V_o}{E^*} \times 100\%$	0.0025	3.6
$\frac{\omega^* - \omega}{\omega^*} \times 100\%$	0.015	0.13
P1	11.67 W	10.8 W
P2	5.764 W	5.4 W
Q1	–4.652 Var	–4.335 VAr
Q2	–2.354 Var	–2.155 VAr

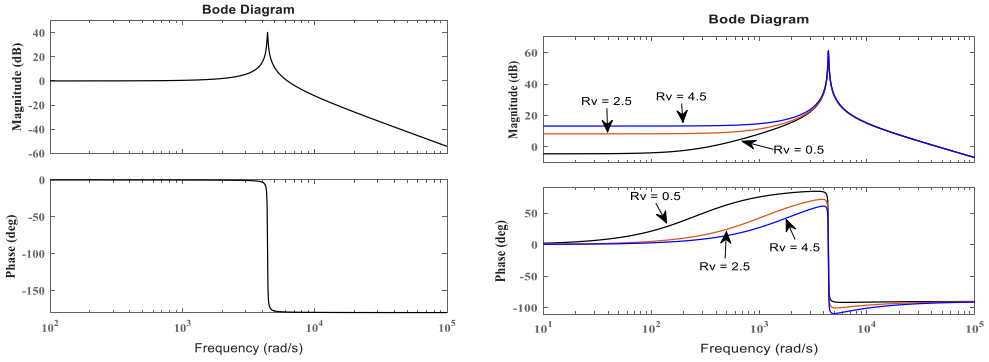

(i) (ii)

Fig. 9. (i) Magnitude and phase plots of G_f(s) (ii) Magnitude and phase plots of $Z_{eff}(s)$ for different values of virtual resistance.

Instead of forming state space matrix, A_{PRO}, a fourth order polynomial is formed in 's'. The location of roots of the polynomial on the complex plane reflects the transient performance of the VSI. A fourth order polynomial takes the following form [17].

$$as^4 + bs^3 + cs^2 + ds + e = 0 \tag{35}$$

The coefficients from a to e are not provided due to space limit.

2.6.2. Selection criteria of virtual resistor, R_v

A 50 Hz, 1-Φ VSI, shown in Fig. 2, connected to a constant impedance load, is considered. The frequency and phase plots of $Z_{eff}(s)$ and G_f(s) are drawn by using data in Table 1 for determining the desired value of the virtual resistance, R_v. The description of $Z_{eff}(s)$ (effective output impedance of inverter) and G_f(s) (transfer function) are given in (36). It can be observed from the plots in Fig. 9(ii) that increasing R_v causes the Z_{eff} to become more resistive at the fundamental frequency. Along with this, the magnitude of Z_{eff} also increases and that can degrade the voltage quality in case of non linear loads. Therefore, a compromise has to be made between desired resistive characteristics and magnitude of Z_{eff} [18].

$$G_f(s) = \frac{1}{C_f L_f s^2 + C_f r_f s + 1}, \quad Z_{eff}(s) = R_v G_f(s) + Z_{th}(s) = \frac{L_f s + r_f + R_v}{C_f L_f s^2 + C_f r_f s + 1} \tag{36}$$

$Z_{th}(s)$ - Thevenin's impedance transfer function

C_f, L_f and r_f are parameters associated with filter circuit of inverter. R_v is the virtual resistor used in the control scheme (refer Fig. 8).

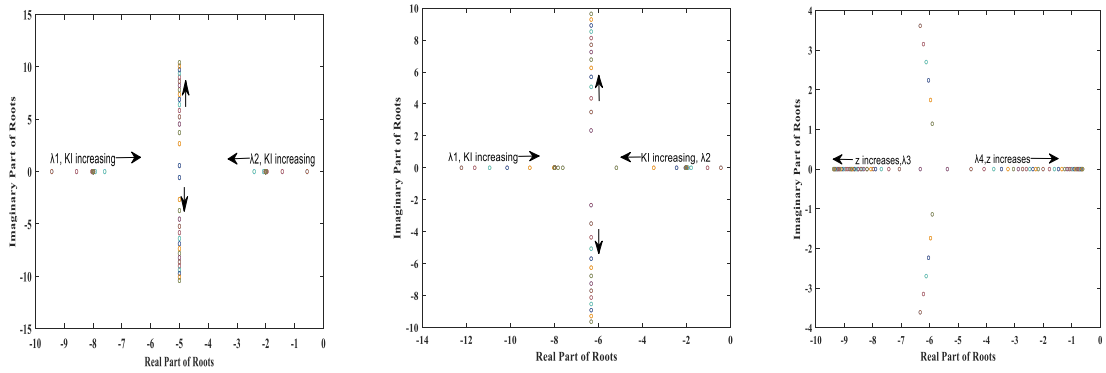

Fig. 10. (i) Location of eigenvalues for variation in K_I, (K_P = 0) (ii) Location of eigenvalues for variation in K_I, (K_P = 0.5) (iii) Location of roots for variation in load resistor.

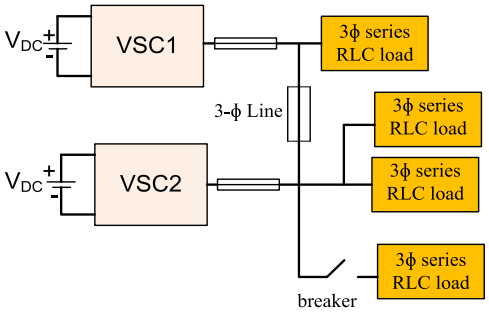

Fig. 11. Standard microgrid setup.

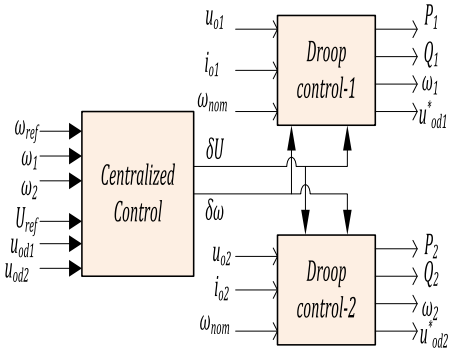

Fig. 12. Centralized secondary control.

2.6.3. Eigenvalue analysis

The dynamic response of small signal model of VSI depend on the location of roots on the complex plane. All the four roots (λ_1–λ_4) have negative real part when $K_I = 1$ and $K_P = 0$. The traces of polynomial roots are shown in Fig. 10(i) when K_I increases from 1 and K_P is zero. The real part of two roots (λ_1 and λ_2) come closer to each other on the real axis and splits into the complex pair roots making the dynamic response faster. In an another Fig. 10(ii), $K_P = 0.5$ increases the damping of the dynamic response of VSI. The roots λ_3 and λ_4 are operating point dependent, which changes their location on the complex plane when load (resistor) increases from 9 Ω to 25 Ω as shown in Fig. 10(iii).

2.7 Centralized secondary control

The concept of centralized secondary control in microgrid operation is described with various submodels, presented in this subsection. The microgrid setup, shown in Fig. 11 is considered for illustration. Two voltage source converters are connected to bus loads through feeder-1 and feeder-2. These feeders are connected with each other through a 3-Φ line. An additional load can be connected at the bus-2 by operation of a breaker switch. The centralized secondary control block, shown in Fig. 12, computes the deviation in voltage and frequency. The signals U^*(reference voltage) and mean of u_{od1} and u_{od2} are compared and the resulting signal is processed through a PI controller to generate u_{PI}. Likewise, the signal ω_{PI} is generated. These deviations are fed to the corresponding droop control blocks of inverters, participating in the parallel operation. Subsequently, in the voltage control model, the d-axis reference signals (u^*_{od}), resulting from the droop controller blocks, are compared with the sampled output signals to reduce the errors. The detail of voltage and current control models are described in the subsequent sub sections [27–30].

2.7.1. Power sharing controller

The basic idea of power sharing function is to balance any change in load by either decreasing or increasing frequency and voltage magnitude of the system according to the droop equations. Instantaneous active and reactive power are calculated by means of output voltage and current measured through *d-q* transformation

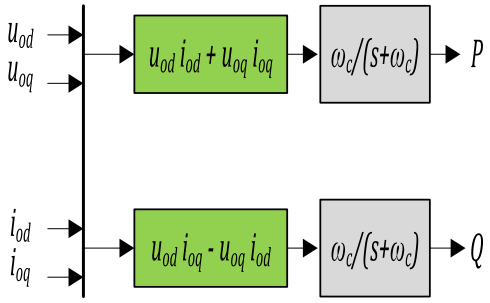

Fig. 13. Power calculation scheme.

block. Low pass filter is used in the power calculation scheme, shown in Fig. 13 in order to extract its fundamental component [27].

$$P = \frac{\omega_c}{s + \omega_c}(u_{od}i_{od} + u_{oq}i_{oq}) \tag{37}$$
$$Q = \frac{\omega_c}{s + \omega_c}(u_{od}i_{oq} - u_{oq}i_{od})$$

In (37), ω_c is the cutoff frequency of the low pass filter, u_{od}, i_{od}, u_{oq} and i_{oq} are the d and q axis components of output voltage and current. Therefore, the small signal dynamic model of the power controller is expressed by (38) and (39).

$$\Delta\dot{P} = -\omega_c\Delta P + \omega_c(I_{od}\Delta u_{od} + I_{oq}\Delta u_{oq} + U_{od}\Delta i_{od} + U_{oq}\Delta i_{oq}) \tag{38}$$

$$\Delta\dot{Q} = -\omega_c\Delta Q + \omega_c(I_{oq}\Delta u_{od} - I_{od}\Delta u_{oq} - U_{oq}\Delta i_{od} + U_{od}\Delta i_{oq}) \tag{39}$$

Where $\dot{P} = \frac{\partial P}{\partial t}$; $\Delta\dot{P}$ and $\Delta\dot{Q}$ denotes small perturbation of state variables P and Q around nominal operating point. U_{odq} and I_{odq} are d-q axis output voltages and currents respectively at steady operating points. The combination of (38) and (39) constitutes the small signal model of power sharing block.

The d-axis droop equations are expressed by (40) and (42).

$$u_{od}^* = U^* - n_cQ - u_{dvir} - u_{PI} \tag{40}$$

Where, $u_{dvir} = i_{oq}X_v + i_{od}R_v$

$$u_{oq}^* = 0 \tag{41}$$

$$\omega = \omega^* - m_cP - \omega_{PI} \tag{42}$$

Where m_c, n_c are droop gains; X_v, R_v are virtual reactance and resistance coupled to the d-axis; U^*, ω^* are the nominal voltage and frequency of the system. The small signal model of droop control is described as given below.

$$\Delta u_{od}^* = -n_c\Delta Q - (\Delta i_{oq}X_v + \Delta i_{od}R_v) - \Delta u_{PI} \tag{43}$$

$$\Delta u_{oq}^* = 0 \tag{44}$$

$$\Delta\omega = -m_c\Delta P - \Delta\omega_{PI} \tag{45}$$

It is notable that droop characteristics, in Eqs. (40) and (42) are defined for predominantly inductive inverter. On the other hand, these equations differ in Subsection 2.1 due to resistive nature of inverter output impedance. To convert variables from each inverter's reference to a common frame, the angle difference between each inverter's d-q frame and the common D-Q frame is specified in Eq. (46).

$$\delta = \int (\omega - \omega_{com})dt \tag{46}$$

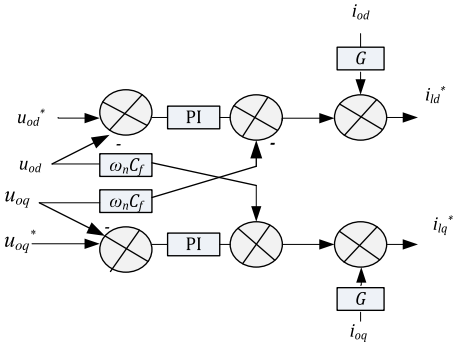

Fig. 14. Voltage controller model.

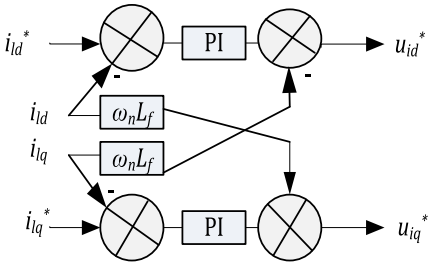

Fig. 15. Current controller model.

Where ω_{com} is the angular frequency of common reference frame adopted by first inverter. Therefore, the small signal model is given in (47).

$$\dot{\Delta\delta} = \Delta\omega - \Delta\omega_{com} = -m_c \Delta P - \Delta\omega_{com} \tag{47}$$

2.7.2. Voltage controller model

The voltage control loop uses a standard proportional and integral (PI) regulator, as illustrated in Fig. 14, which compares the sampled output voltage with the reference value provided by the power controller to obtain a feed-forward gain to account for output current disturbance and generate the reference decoupling current. The state space equations of the voltage control model are stated as follows [27, 28].

$$\frac{d\Phi_d}{dt} = u_{od}^* - u_{od} \tag{48}$$

$$\frac{d\Phi_q}{dt} = u_{oq}^* - u_{oq} \tag{49}$$

$$i_{ld}^* = K_{iu}\Phi_d + K_{pu}(u_{od}^* - u_{od}) - \omega_n C_f u_{oq} + G i_{od} \tag{50}$$

$$i_{lq}^* = K_{iu}\Phi_q + K_{pu}(u_{oq}^* - u_{oq}) + \omega_n C_f u_{od} + G i_{oq} \tag{51}$$

Where K_{iu} and K_{pu} are integral and proportional gains of PI controller respectively, G being the feedforward gain; C_f is per phase capacitance of LC filter. The small signal model can now be given as follows.

$$\Delta\dot{\Phi}_d = \Delta u_{od}^* - \Delta u_{od} \tag{52}$$

$$\Delta\dot{\Phi}_q = \Delta u_{oq}^* - \Delta u_{oq} \tag{53}$$

Therefore, (50) and (51) are expressed as

$$\Delta i_{ld}^* = K_{iu}\Delta\Phi_d + K_{pu}(\Delta u_{od}^* - \Delta u_{od}) - \omega_n C_f \Delta u_{oq} + G\Delta i_{od} \tag{54}$$

$$\Delta i_{lq}^* = K_{iu}\Delta\Phi_q + K_{pu}(\Delta u_{oq}^* - \Delta u_{oq}) + \omega_n C_f \Delta u_{od} + G\Delta i_{oq} \tag{55}$$

2.7.3. Current controller model

The current controller, similar to the voltage control loop, produces the SPWM (sinusoidal pulse width modulation) signal by comparing the sampled filter current with the reference value provided by the voltage controller (in Fig. 14) via a PI controller. This method yields the least current error [28, 29]. The small signal model is described in Eqs. (56) to (59).

$$\Delta\dot{\Upsilon}_d = \Delta i_{ld}^* - \Delta i_{ld} \tag{56}$$

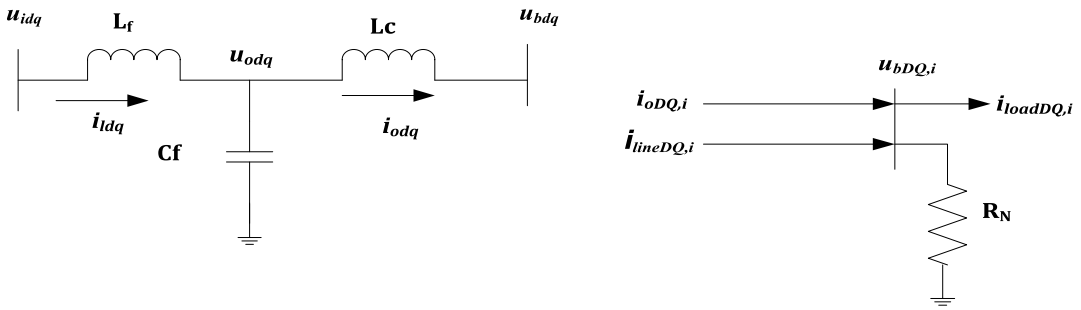

Fig. 16. (i) LCL Filter model (ii) Insertion of R_N.

$$\Delta\dot{\Upsilon}_q = \Delta i^*_{lq} - \Delta i_{lq} \tag{57}$$

$$\Delta u^*_{id} = K_{ic}\Delta\Upsilon_d + K_{pc}(\Delta i^*_{ld} - \Delta i_{ld}) - \omega_n L_f \Delta i_{lq} \tag{58}$$

$$\Delta u^*_{iq} = K_{ic}\Delta\Upsilon_q + K_{pc}(\Delta i^*_{lq} - \Delta i_{lq}) + \omega_n L_f \Delta i_{ld} \tag{59}$$

Where K_{ic} and K_{pc} are integral and proportional gains of PI controller respectively; L_f being the per phase inductance of LC filter; i_{ld}, i_{lq} are the filter currents in *d-q* reference frame. The current control scheme is shown in Fig. 15.

2.7.4. LC filter and coupling inductance model

The diagram of LCL filter is shown in Fig. 16(i). Without any loss of inaccuracies, it is assumed that the $u^*_{idq} = u_{idq}$. The state equations of filter dynamics are given as [29, 31]

$$\dot{i_{ld}} = \frac{1}{L_f}\left(-R_f i_{ld} + u_{id} - u_{od}\right) + \omega_0 i_{lq} \tag{60}$$

$$\dot{i_{lq}} = \frac{1}{L_f}(-R_f i_{lq} + u_{iq} - u_{oq}) - \omega_0 i_{ld} \tag{61}$$

$$\dot{i_{od}} = \frac{1}{L_c}(-R_c i_{od} + u_{od} - u_{bd}) + \omega_0 i_{oq} \tag{62}$$

$$\dot{i_{oq}} = \frac{1}{L_c}(-R_c i_{oq} + u_{oq} - u_{bq}) - \omega_0 i_{od} \tag{63}$$

$$\dot{u_{od}} = \frac{1}{C_f}(i_{ld} - i_{od}) + \omega_0 u_{oq} \tag{64}$$

$$\dot{u_{oq}} = \frac{1}{C_f}(i_{lq} - i_{oq}) - \omega_0 u_{od} \tag{65}$$

The small signal model can be obtained as follows by taylor expansion to the dynamic model presented in (60) to (65) [28, 31]

$$\Delta\dot{i_{ld}} = \frac{1}{L_f}(\Delta u_{id} - \Delta u_{od}) - \frac{R_f}{L_f}\Delta i_{ld} + \omega_0 \Delta i_{lq} + I_{lq}\Delta\omega_0 \tag{66}$$

$$\Delta\dot{i_{lq}} = \frac{1}{L_f}(\Delta u_{iq} - \Delta u_{oq}) - \frac{R_f}{L_f}\Delta i_{lq} + \omega_0 \Delta i_{ld} + I_{ld}\Delta\omega_0 \tag{67}$$

$$\Delta\dot{i_{od}} = \frac{1}{L_c}(\Delta u_{od} - \Delta u_{bd}) - \frac{R_c}{L_c}\Delta i_{od} + \omega_0 \Delta i_{0q} + I_{0q}\Delta\omega_0 \tag{68}$$

$$\Delta\dot{i_{oq}} = \frac{1}{L_c}(\Delta u_{oq} - \Delta u_{bq}) - \frac{R_c}{L_c}\Delta i_{oq} - \omega_0 \Delta i_{0d} - I_{0d}\Delta\omega_0 \tag{69}$$

$$\Delta\dot{u}_{od} = \frac{1}{C_f}(\Delta i_{ld} - \Delta i_{od}) + \omega_0 \Delta u_{oq} + U_{oq}\Delta\omega_0 \tag{70}$$

$$\Delta\dot{u}_{oq} = \frac{1}{C_f}(\Delta i_{lq} - \Delta i_{oq}) - \omega_0 \Delta u_{od} - U_{od}\Delta\omega_0 \tag{71}$$

Where u_{id}, u_{iq} are the inverter voltages in d-q frame; u_{bd} and u_{bq} are the d-q axis bus voltages; u_{od}, u_{oq} are d-q axis output voltages; i_{ld}, i_{lq} are d-q axis line currents; ω_o is steady state value of frequency at initial operating point. I_{ldq} refers to d-q axis filter current at steady operating point.

2.7.5. Complete model of DG interface

Output variables i_{odq} and input variables u_{bdq} can be transformed to common d-q reference frame using transformation matrix given below.

$$[i_{oDQ}] = [T][i_{odq}] \tag{72}$$

$$[u_{bdq}] = [T^{-1}][u_{bDQ}] \tag{73}$$

Where $T = \begin{bmatrix} \cos\delta & -\sin\delta \\ \sin\delta & \cos\delta \end{bmatrix}$, $T^{-1} = \begin{bmatrix} \cos\delta & \sin\delta \\ -\sin\delta & \cos\delta \end{bmatrix}$,

Combining all state space models from (38) to (72), a thirteen state variables of a single inverter are chosen and an output equation in common frame can be obtained as follows [27].

$$[\Delta\dot{x_{invi}}] = A_{INVi}[\Delta x_{invi}] + B_{INVi}[\Delta u_{bDQ}] + B_{i\omega com}[\Delta\omega_{com}] \tag{74}$$

$$\begin{bmatrix} \Delta\omega_i \\ \Delta i_{oDQi} \end{bmatrix} = \begin{bmatrix} C_{INV\omega i} \\ C_{INVci} \end{bmatrix}[\Delta x_{invi}] \tag{75}$$

Where $[\Delta x_{invi}] = [\Delta\delta_i\ \Delta P_i\ \Delta Q_i\ \Delta\Phi_{di}\ \ \Delta\Phi_{qi}\ \ \Delta\Upsilon_{di}\ \Delta\Upsilon_{qi}\ \Delta i_{ldi}\ \Delta i_{lqi}\ \Delta u_{odi}\ \Delta u_{oqi}\ \Delta i_{odi}\ \Delta i_{oqi}]_{1\times 13}$

2.7.6. Model of two parallel inverters

The procedural steps of small signal model of two inverters, connected in parallel, can be obtained as follows based on single inverter model [27, 31].

$$[\Delta\dot{x_{INV}}] = A_{INV}[\Delta x_{INV}] + B_{INV}[\Delta u_{bDQ}] \tag{76}$$

$$[\Delta i_{oDQ}] = C_{INVc}[\Delta x_{INV}] \tag{77}$$

Where $[\Delta x_{INV}] = [x_{inv1}\ x_{inv2}]^T$, $[\Delta u_{bDQ}] = [\Delta u_{bDQ1}\ \Delta u_{bDQ2}]^T$

$$A_{INV} = \begin{bmatrix} A_{INV1} + B_{1\omega com}C_{INV\omega 1} & 0 \\ B_{2\omega com}C_{INV\omega 1} & A_{INV2} \end{bmatrix}$$

$$B_{INV} = \begin{bmatrix} B_{INV1} & 0 \\ 0 & B_{INV2} \end{bmatrix}, \quad C_{INVc} = \begin{bmatrix} C_{INV1} & 0 \\ 0 & C_{INV2} \end{bmatrix}$$

D matrix is not present in the output state space matrix, given in 77. This is due to involved system dynamics. The more simple explanation lies in the fact that output takes time to change when input changes.

2.7.7. Network and load model

The small signal model of network and load can be obtained in a way similar to the LCL filter linearization process. The nonlinear differential equation of line current of ith line, on a common reference frame, connected between nodes j and k are expressed as [31].

$$\frac{di_{lineDi}}{dt} = \frac{-r_{linei}}{L_{linei}} i_{lineDi} + \omega i_{lineQi} + \frac{1}{L_{linei}} u_{bDj} - \frac{1}{L_{linei}} u_{bDk} \tag{78}$$

$$\frac{di_{lineQi}}{dt} = \frac{-r_{linei}}{L_{linei}} i_{lineQi} - \omega i_{lineDi} + \frac{1}{L_{linei}} u_{bQj} - \frac{1}{L_{linei}} u_{bQk} \tag{79}$$

Now, linearizing (78) and (79) around steady state point, results in Eq. (80). In the same way, for load at i^{th} node, linearized model of load can be expressed in (83).

$$[\Delta \dot{i}_{lineDQ}] = A_{NET}[\Delta i_{lineDQ}] + B_{1NET}[\Delta u_{bDQ}] + B_{2NET}[\Delta \omega] \tag{80}$$

The nonlinear differential equation for load (resistive-inductive type) model, at i^{th} node is

$$\frac{di_{loadDi}}{dt} = \frac{-R_{loadi}}{L_{loadi}} i_{loadDi} + \omega i_{loadQi} + \frac{1}{L_{loadi}} u_{bDj} \tag{81}$$

$$\frac{di_{loadQi}}{dt} = \frac{-R_{loadi}}{L_{loadi}} i_{loadQi} - \omega i_{loadDi} + \frac{1}{L_{loadi}} u_{bQj} \tag{82}$$

$$[\Delta \dot{i}_{loadDQ}] = A_{Load}[\Delta i_{loadDQ}] + B_{1load}[\Delta u_{bDQ}] + B_{2load}[\Delta \omega] \tag{83}$$

Where $A_{NET} = \begin{bmatrix} -\frac{R_{line1}}{L_{line1}} & \omega_o \\ -\omega_o & -\frac{R_{line1}}{L_{line1}} \end{bmatrix} 2n \times 2n$

$$B_{1NET} = \begin{bmatrix} \frac{1}{L_{line1}} & 0 & -\frac{1}{L_{line1}} & 0 \\ 0 & \frac{1}{L_{line1}} & 0 & -\frac{1}{L_{line1}} \end{bmatrix}_{2\times 2m}, B_{2NET} = [i_{lineQ1} - i_{lineD1}]^T_{1\times 2n}$$

A_{Load}, B_{1Load} and B_{2Load} matrices can be obtained in almost the same way as network model. The detail of matrices B_{INVi}, $B_{i\omega com}$, $C_{INV\omega i}$ and C_{INVci} can be obtained from Appendix A.

2.7.8. Complete microgrid model

When bus voltages are employed as inputs to the system, the consequences of load disturbance cannot be predicted accurately. The system's only disturbance is caused by a step shift in load. As a result, a method is necessary to include bus voltage terms in the system matrix A_{INVi}. This is performed by inserting a virtual resistor (high value) r_N at inverter bus, shown in Fig. 16(ii) [27–30]. The small signal model is obtained as follows.

$$[u_{bDQ}] = R_N(M_{INV}[\Delta i_{oDQ}] + M_{Load}[\Delta i_{LoadDQ}] + M_{NET}[\Delta i_{lineDQ}]) \tag{84}$$

M_{INV}, M_{Load} and M_{NET} are the matrices which map DG connection points, load connection points and connecting lines onto network nodes respectively. If i^{th} inverter is connected at j^{th} node point then $M_{INV}(j,i) = 1$ and all other elements in that row are zero. In M_{NET} matrix, +1 or –1 should be carefully put based on whether line current is entering or leaving the node. Now, in Fig. 11, the microgrid structure consists of $n = 1$ line, $s_{DG} = 2$ DGs, $p = 2$ Loads and $m = 2$ nodes. A 32 ($=2n + 2p + 13s_{DG}$) order small signal model of

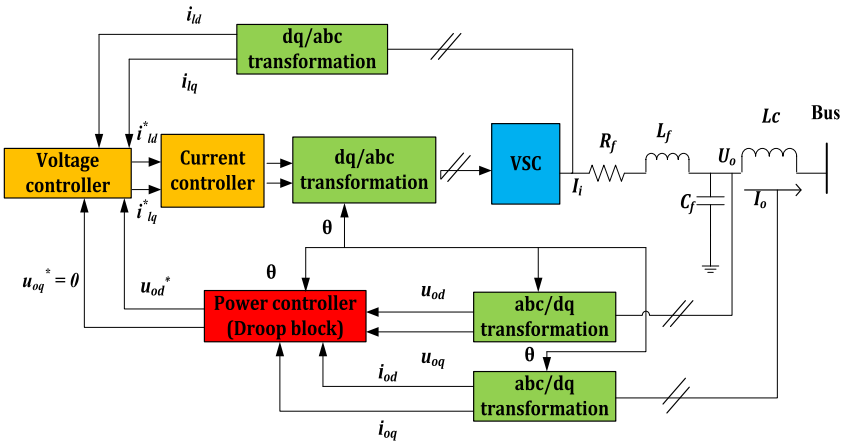

Fig. 17. Inverter based microgrid controls [23].

Fig. 11 can be obtained and given by (85).

$$\begin{bmatrix} \Delta\dot{x}_{INV} \\ \Delta\dot{i}_{lineDQ} \\ \Delta\dot{i}_{loadDQ} \end{bmatrix} = A_{MG} \begin{bmatrix} \Delta x_{INV} \\ \Delta i_{lineDQ} \\ \Delta i_{loadDQ} \end{bmatrix} \tag{85}$$

The matrix A_{MG} is used to find the modes or eigenvalues of the system.

$$\text{Where} \begin{bmatrix} \Delta x_{INV} \\ \Delta i_{lineDQ} \\ \Delta i_{loadDQ} \end{bmatrix} = [\Delta\delta_1 \Delta P_1 \Delta Q_1 \Delta\Phi_{d1}\ \Delta\Phi_{q1}\ \Delta\Upsilon_{d1}\ \Delta\Upsilon_{q1}\ \Delta i_{ld1}\ \Delta i_{lq1}\ \Delta u_{od1}\ \Delta u_{oq1}\ \Delta i_{od1}\ \Delta i_{oq1}\ \Delta\delta_2 \Delta P_2 \Delta Q_2$$

$$\Delta\Phi_{d2}\ \Delta\Phi_{q2}\ \Delta\Upsilon_{d2}\ \Delta\Upsilon_{q2}\ \Delta i_{ld2}\ \Delta i_{lq2}\ \Delta u_{od2}\ \Delta u_{oq2}\ \Delta i_{od2} \Delta i_{oq2}\ \ \Delta i_{lineD1} \Delta i_{lineQ1}\ \Delta i_{loadD1} \Delta i_{loadQ1} \Delta i_{loadD2} \Delta i_{loadQ2}]^T_{(1\times 32)}$$

$$M_{NET} = \begin{bmatrix} -1 & 0 \\ 0 & -1 \\ 1 & 0 \\ 0 & 1 \end{bmatrix}_{2m\times 2n} \quad R_N = \begin{bmatrix} R_N & 0 & 0 & 0 \\ 0 & R_N & 0 & 0 \\ 0 & 0 & R_N & 0 \\ 0 & 0 & 0 & R_N \end{bmatrix}_{2m\times 2m} \quad M_{INV} = \begin{bmatrix} 1 & 0 & 0 & 0 \\ 0 & 1 & 0 & 0 \\ 0 & 0 & 1 & 0 \\ 0 & 0 & 0 & 1 \end{bmatrix}_{2m\times 2s_{DG}}$$

$$M_{Load} = \begin{bmatrix} -1 & 0 & 0 & 0 \\ 0 & -1 & 0 & 0 \\ 0 & 0 & -1 & 0 \\ 0 & 0 & 0 & -1 \end{bmatrix}_{2m\times 2p}$$

The combined model of inverter control, with its components, is shown in Fig. 17. R_f, L_f and C_f are the filter parameters; L_c is the coupling inductor respectively. As illustrated, the angle (θ), which is derived from the integration of the angular frequency (ω), is used to convert the three-phase output voltage and current to their *d-q* frame components.

2.7.9. Method of virtual impedance

Virtual impedance is an artificially created impedance in the inverter control block to resolve the issues of inverter feeder line asymmetry, proportionate reactive power sharing among inverters etc in the microgrid operations [21–23]. In an islanded mode of operation, maintaining voltage and frequency within specified limits has been remain a challenge. The microsource inverters use droop control, described in 40 and 42 to decentrally regulate active and reactive powers. The active power is shared in proportion to the inverter's capacity as frequency is a global variable in the MG configuration. On the other hand, sharing of reactive power is often found erroneous due to mismatch in the bus voltages as these work as a local variable. The virtual impedance is suggested as a means to solve this issue by balancing the feeder line impedances. The method to design R_v and X_v is described in the flowchart shown in Fig. 18 [29, 30].

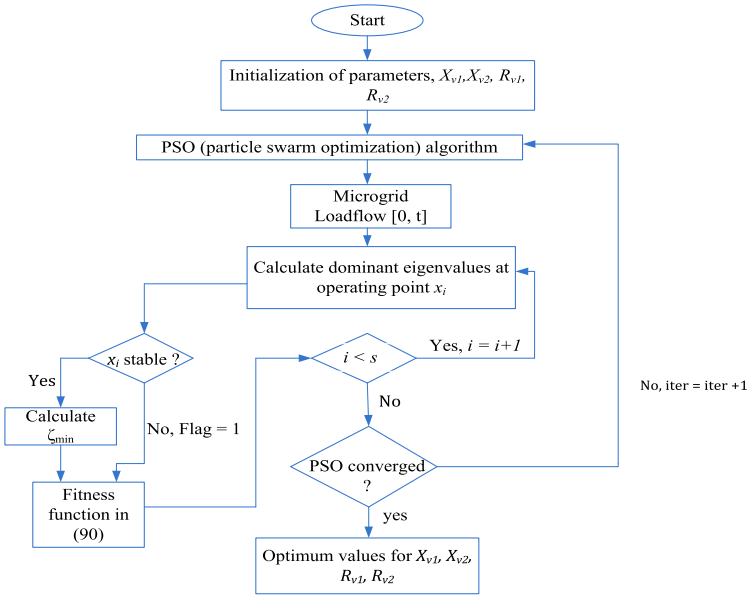

Fig. 18. Flowchart to design VI.

Each microgrid has its X_v and R_v parameters. In order to estimate these parameters, a fitness function is defined with an objective of minimizing the reactive power sharing error between VSIs and to maximize the damping of dominant eigenvalue. The Particle Swarm Optimization algorithm is used to optimize the fitness function. The damping ratio of a mode or eigenvalue is defined as-

$$\text{Damping ratio } (\zeta) = \frac{\text{abs(real)}}{\sqrt{\text{real}^2 + \text{imag}^2}}, \tag{86}$$

Where '*real*' refers to the real part of dominant eigenvalue and '*imag*' refers to the imaginary part. The minimum damping ratio of dominant eigenvalues at i^{th} operating point is-

$$\zeta_{min}{}^{i} = [\zeta_1, \zeta_2, \zeta_3, \ldots.. \zeta_k] \tag{87}$$

k is the number of dominant eigenvalue at i^{th} operating point. The minimum damping in *s* operating points is-

$$\zeta_{min} = [\zeta_{min}^1, \zeta_{min}^2, \zeta_{min}^3, \ldots.. \zeta_{min}{}^{s}] \tag{88}$$

The per unit reactive power mismatch between two inverters is computed by (89).

$$\Delta Q = \sum_{k=1}^{1} abs\ (n_k Q_k - n_{k+1} Q_{k+1}) \tag{89}$$

The fitness function is defined in (90) by considering the reactive power mismatch and enhancing the small signal stability of MG.

$$\text{Fitness function} = \Delta Q(1 - \zeta_{\min}), \tag{90}$$

Subjected to Constraints, $0 < \zeta_{min} < 1$ and $1.05\ p.u < u_{odi} < 0.95\ p.u$, $i = 1,2$

The minimization of fitness function, described in (90) ensures minimum reactive power sharing error with enhanced small signal stability.

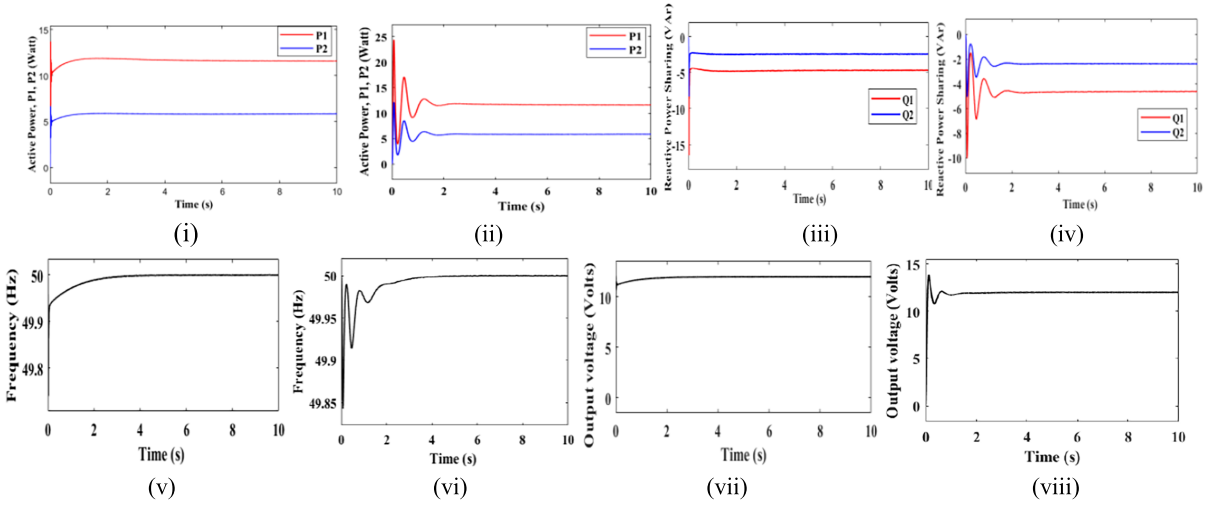

Fig. 19. (i) Active power sharing (P1, P2) vs time with K_p = 0.5 (ii) Active power sharing (P1, P2) vs time with K_p = 0 (iii) reactive power sharing (Q1, Q2) vs time with K_p = 0.5 (iv) reactive power sharing (Q1, Q2) vs time with K_p = 0 (v) system frequency vs time with K_p = 0.5 (vi)) system frequency vs time with K_p = 0 (vii) RMS o/p voltage vs time with K_p = 0.5 and (viii) RMS o/p voltage vs time with K_p = 0.

3. Result and discussion

3.1. Simulation results of transient droop characteristics enabled inverter

The system parameters for simulation of model /scheme are shown in Table 1. Coefficients n and m are selected on the basis of voltage drop ratio ($\frac{nP^*}{E^*K_e}$) and frequency boost ratio ($\frac{mQ^*}{\omega^*}$) at rated power respectively.

3.1.1. Scenario-1

Two inverters ($i = 1,2$) of rating 50 VA and 25 VA are considered for parallel operation with a nonlinear load (diode based rectifier with LC filter, L_{fL} = 150 mH, C_{fL} = 1000 μF, R_L = 9 Ω) connected across load terminals. In this scenario, modified robust droop control structure is considered for the system of two inverters operating in parallel. Two cases (K_p = 0.5 and K_p = 0) with modified structure are compared. The output voltage, system frequency, reactive and active power sharing, RMS output voltage are demonstrated in Fig. 19. It is observed that system responses with K_p = 0.5 have good dynamic response in terms of less over/undershoots settling time etc. The deviation in the output voltage and frequency from their nominal values are either zero or close to zero at the steady state. The reactive and active powers are shared in the ratio of power rating (2:1) of two inverters.

Next, in the Fig. 20, responses are shown when robust droop control scheme is not equipped with the proposed method. In Fig. 20(iii) and (iv), there has been deviation (0.45 Volt from nominal in V_{oRMS}, 0.07 Hz from nominal in frequency) in the steady state RMS output voltage and frequency for the obvious reasons mentioned in Subsection 2.2.

The % error in the o/p voltage and system frequency are computed and shown for both cases *i.e* with and without compensation, in Table 2.

3.1.2. Scenario-2

The scenario-2 consists of same system of inverters, connected to a linear load of 18 Ω initially. The modified structure of robust droop control is considered with K_p = 0.5. At t = 5 sec, the ohmic value of load is reduced (halved) to 9 Ω. It is observed from the responses, shown in Fig. 21 that in the steady state, reactive and active power are shared in proportion to the power ratings of inverters *i.e* $\frac{P1}{P2} = \frac{2}{1}$, $\frac{Q1}{Q2} = \frac{2}{1}$, before and after the switching. In the steady state, there is no deviation seen in either output voltage or system frequency and this proves the efficacy of the suggested approach.

3.2. Simulation results of centralized secondary control

Three phase series RL load (5800 W and 200 Var at bus-2) is switched (connected) at t = 3 sec and removed at t = 5 sec. The waveforms of power, frequency and voltage, shown in Fig. 22, are observed. At t = 3 s,

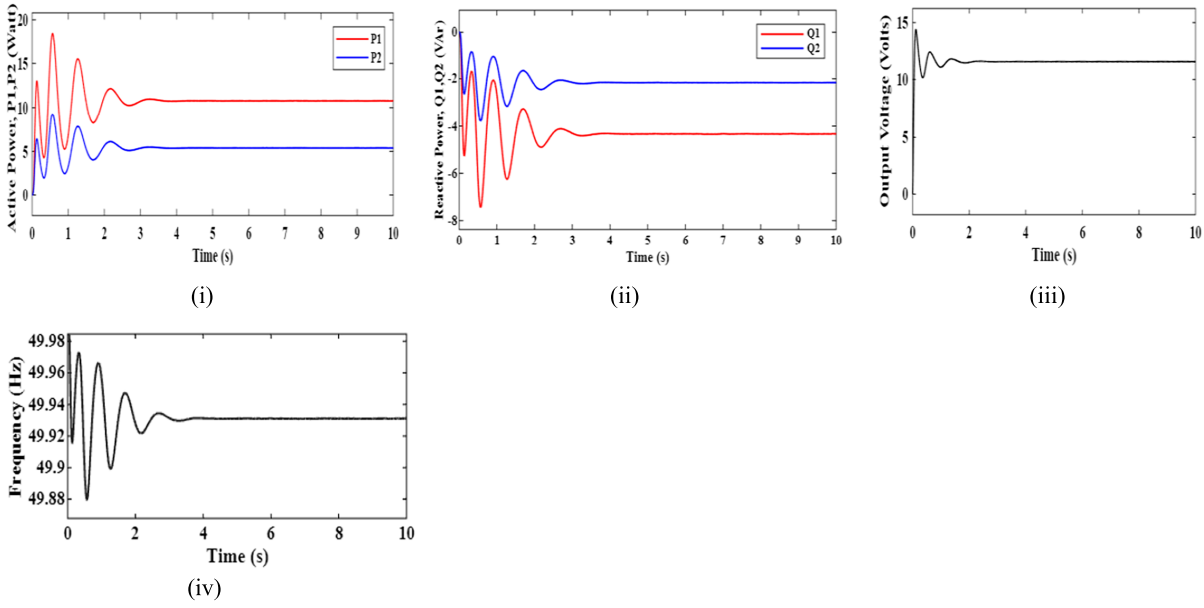

Fig. 20. (i) Active power sharing (P1,P2) vs time (ii) reactive power sharing (Q1,Q2) vs time (iii) RMS o/p voltage vs time (iv) frequency vs time.

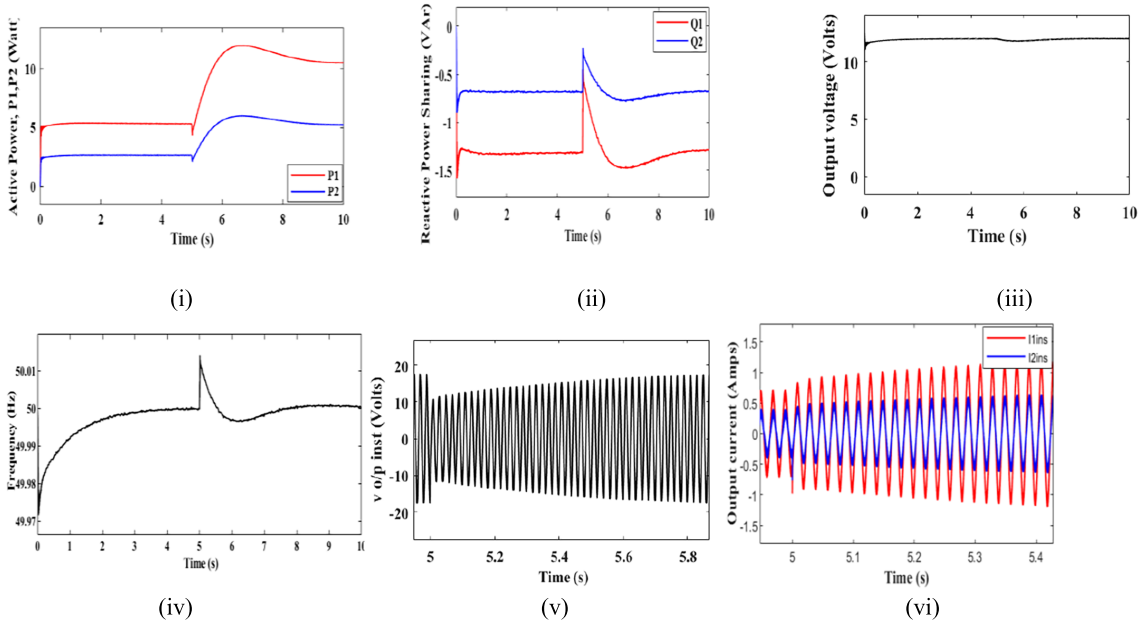

Fig. 21. (i) Active power sharing (P1,P2) vs time (ii) reactive power sharing (Q1,Q2) vs time (iii) RMS o/p voltage vs time (iv) system frequency vs time (v) instantaneous output voltage vs time (vi) instantaneous output current ($i_{1\text{ins}}$, $i_{2\text{ins}}$) vs time.

when Load power (Watt and VAr) is increased, frequency dips but attains steady nominal value (50 Hz) after secondary control activates. The average of the d-axis reference voltages (u_{od1} and u_{od2}) is restored to the nominal value. It is noticeable here, that the reactive power supplied by inverters has different values in spite of same occupying capacity of inverters. This error can be reduced by the method of virtual impedance, applied on the droop control block as already described in Subsection 2.7. The reduction in the reactive power error is demonstrated in Fig. 23(i) and (ii) respectively. The computed virtual reactance values are shown in Table 3. In this study, R_{vi} (i = *1,2*) in $Z_{vi} = R_{vi} + \text{j}\, X_{vi}$, is considered zero.

Table 3. Computed virtual reactance values.

Operating condition	X_{v1} (Ω)	X_{v2} (Ω)
Before Load switching	0.285	0.2
When Load is switched	0.785	0.4

Table 4. Microgrid parameters for simulation.

Parameter	value	units
L C filter	0.1, 3.5, 50	Ω, mH, ìF
Feeder line	0.05, 3.5×10^{-4}	Ω, H
Tie line	0.15, 3.5×10^{-4}	Ω, H
RL Load_1(bus-1)	5800 W, 200	W, VAr
RL Load_2 (bus-2)	8100, 500	W, VAr
Switched RL load (bus-2)	5800, 200	W, VAr
m_c, n_c	9×10^{-6}, 0.003	rad/Watt, V/VAr
U_{ref}	311	V
ω_{ref}	314	rad/s
ω^*	314.16	rad/s
U^*	311.13	Volt
K_{pu}	0.285	
K_{iu}	594.85	
K_{pc}	55	
K_{ic}	1570.8	

Table 5. Steady state operating values.

Parameter	value
u_{od}	[311.2 310.8]
u_{oq}	[–0.4441 –0.2234]
i_{od}	[15 14.84]
i_{oq}	[–0.8653 –0.7866]
i_{Ld}	[15.6 15.54]
i_{Lq}	[3.5 3.762]
i_{LineDQ}	[2.535 –0.3737]
i_{LoadD}	[12.46 17.39]
i_{LoadQ}	[–0.4916 –1.171]
u_{bd}	[310.3 310]
u_{bq}	[–1.923 –2.06]

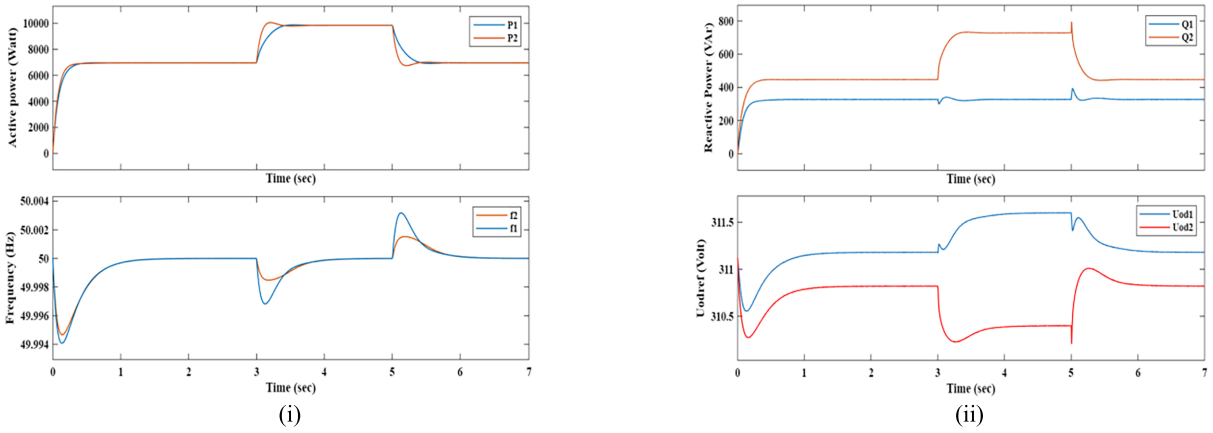

Fig. 22. (i) Active power (P) and frequency (F) restoration (ii) reactive power (Q) and d-axis reference voltage (volt) by secondary control.

The *d-q* axis output currents for two VSIs are shown in Fig. 24(i) followed by line currents in Fig. 24(ii). The *d-q* axis filter currents are shown in Fig. 25. The simulation parameters for this scenario are shown in Table 4. The steady operating values are given in Table 5.

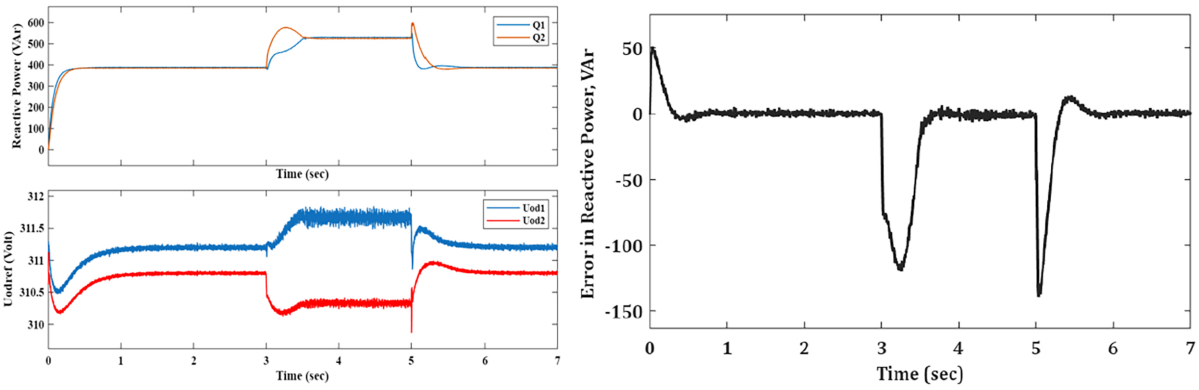

Fig. 23. (i) Reactive power (VAr) and d axis reference voltage (volt) by VI method (ii) Error in reactive power sharing.

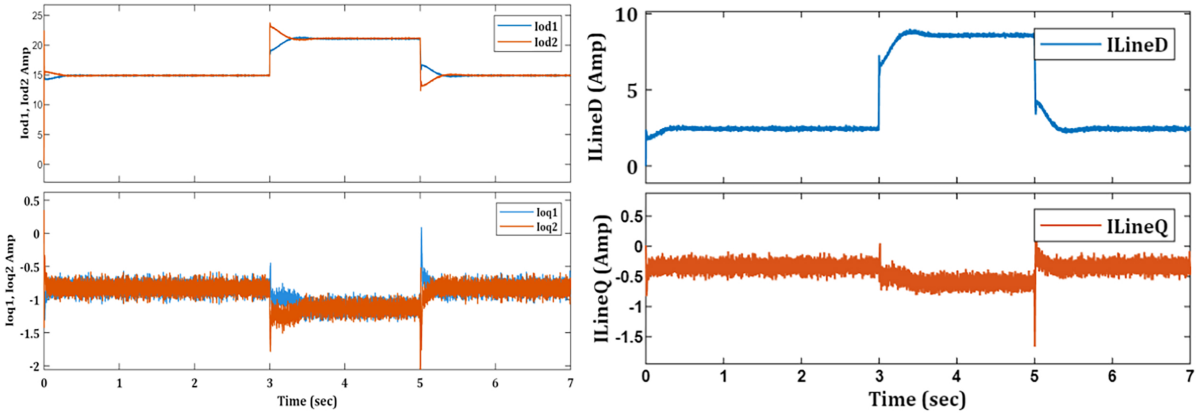

Fig. 24. (i) *d-q* axis output currents (ii) *d-q* axis Line currents.

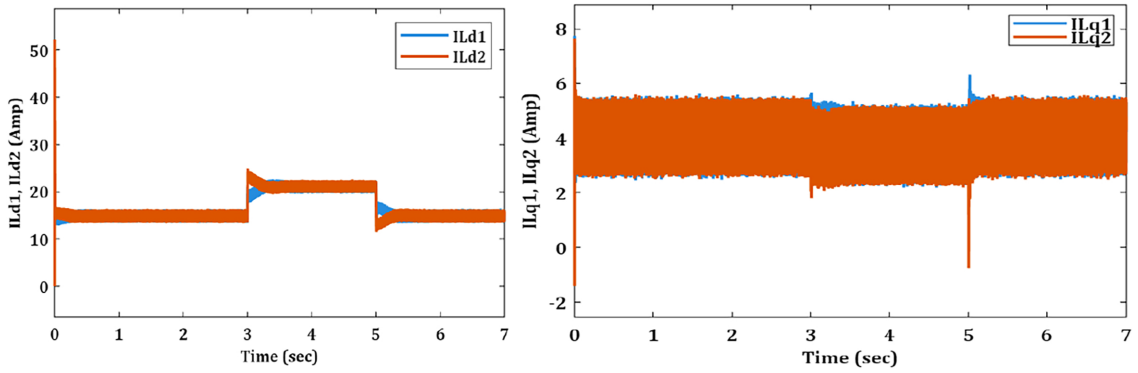

Fig. 25. *d-q* axis filter currents (i) *d* axis (ii) *q* axis.

3.3. Observation

The method of virtual impedance reshapes the reactive power supplied by inverters so that the error between them as depicted in Fig. 23(i) and (ii), is nearly zero. This ensures the proportionate power sharing between inverters. The addition of virtual impedance x_{v1} in the droop control block of inverter-1 makes it softer source enabling more reactive current to flow. At the same time, addition of virtual impedance, $-x_{v2}$ in the droop control block of inverter-2 makes it stiffer source enabling less reactive current to flow. Consequently, inverter-1 supplies more reactive power and inverter-2 supplies less reactive power. This adjustment of tuning x_{v1} and x_{v2} in the control algorithm occurs until reactive power sharing error between two sources is nearly zero. However,

the *d*- axis bus voltages (U_{od1ref} and U_{od2ref}) have a significant difference as shown in Fig. 23(i). This difference justifies the flow of reactive power from bus-1 to bus-2.

4. Conclusion

This paper suggests TDC enabled RDC scheme to compensate/restore the deviations in the output voltage and system frequency. A model of two single phase inverters, operated in parallel and equipped with aforesaid mechanism, is considered for validation. The selection of virtual resistor in the control model of 1-Φ inverter is discussed through transfer function approach. The small signal model is built and damping characteristics is evaluated by eigen value analysis. Similar objectives have been accomplished in a system comprising two 3-Φ voltage source inverters that are coupled to loads via buses and equipped with centralized secondary control. The submodels of the small signal model of inverter-based microgrid control are described. The idea of VI is thoroughly explained with its parameter design algorithm. Simulations validate the models and schemes presented in the study. The future works involve-(i) The issues of harmonic contents in either output voltage or current due to presence of nonlinear load (in RDC scheme) are likely to be addressed. (ii) inclusion of VSG (Virtual Synchronous Generator) with VI, in inverter control block. Additionally, the presented work is likely to be extended experimentally by hardware-in-the-loop testing setups in the future.

Abbreviations

CDC: conventional droop control
MG: microgrid
PI: proportional integral
Φ: phase
VI: Virtual Impedance
VSI: Voltage source inverter
$\mathbf{i}_{odq}$**:** *d-q* axis output current (3-Φ VSI)
$\mathbf{i}_{ldq}$**:** *d-q* axis filter current (3-Φ VSI)
$\mathbf{i}_{LineDQ}$**:** DQ axis line current (3-Φ VSI)
$\mathbf{i}_{LoadDQ}$**:** D-Q axis load current (3-Φ VSI)
$\mathbf{u}_{odq}$: *d-q* axis output voltage (3-Φ VSI)
U* = reference voltage (3-Φ VSI)
$\mathbf{u}^{*}_{dq}$ = *d-q* axis reference voltage calculated by droop block
$\mathbf{u}_{bdq}$ = *d-q* axis bus voltage (3-Φ VSI)
RDC: robust droop control
RMS: root mean square
s: sec
IBMG: Inverter based microgrid
W: watt
VAr: volt-ampere reactive

Acknowledgements

The authors affirm that the work described in this publication was not influenced by any known conflicting financial interests or personal ties. Funding has not been obtained to complete the manuscript's written draft.

Conflict of interest

The authors declare no conflict of interest.

Author contribution statement

S.B. conducted the research and drafted the manuscript; V.S and M.K supervised and provided key suggestions.

Data availability

No datasets are generated or analyzed during the current study.

References

1. IRENA Homepage, https://www.irena.org/publications/2017/Jul/Renewable-Energy-Statistics-2017, (last accessed Feb. 21,2025).
2. Saeed MH, Fangzong W, Kalwar BA, Iqbal S. Review on Microgrids Challenges & Perspectives. IEEE Access. 2021;9:166502–166517.
3. Bhambri S, Kumawat M, Shrivastava V, Agarwal U, Jain NK. The Energy Mix: An Emerging Trend in Distribution System. In: Singh, S.N., Jain, N., Agarwal, U., Kumawat, M. (eds) Optimal Planning and Operation of Distributed Energy Resources. Energy Systems in Electrical Engineering. Springer, Singapore, pp. 11–37.
4. Tayab UB, Roslan MAB, Hwai LJ, Kashif MA. Review of droop control techniques for microgrid. Renewable and sustainable energy reviews. 2017;76:717–727.
5. Lazzarin TB, Bauer GAT, Barbi I. A Control Strategy for Parallel Operation of Single-Phase Voltage Source Inverters: Analysis, Design and Experimental Results. IEEE Transactions On Industrial Electronics. 2013;60(6):2194–2204.
6. Zhong QC, Hornik T. Control of Power Inverters in Renewable Energy and Smart Grid Integration. 1st ed UK: John Wiley and Sons, 2013.
7. Chandorkar CM, Divan MD, Adapa R. Control of Parallel Connected Inverters in Standalone ac Supply Systems. IEEE Transactions On Industry Applications. 1993;29(1):136–143.
8. Bhambri S, Shrivastava V, Kumawat M, Agrawal S. Modelling and Control of Microgrids in an Offgrid Operating Scenario: A Case Study. In: IEEE Region 10 Symposium (TENSYMP), New Delhi, 27–28 September 2024.
9. Bhambri S, Shrivastava V, Kumawat M. A Case Study on Corrective Measures of Secondary Control Assisted Microgrids. International Energy Journal. 2025;25(1A).
10. Chen K, Baran M. Robust Controller for Community Microgrids for Stability Improvement in Islanded Mode. IEEE Transactions on Power Systems. 2022;38(3):2472–2484.
11. Augustine S, Mishra MK, Lakshminarasamma N. Adaptive Droop Control Strategy for Load Sharing and Circulating Current Minimization in Low-Voltage Standalone DC Microgrid. IEEE Transactions on Sustainable Energy. 2015;6(1),132–141.
12. Yao Z, Xiao L. Control of Single-Phase Grid Connected Inverters With Nonlinear Loads. IEEE Transactions on Industrial Electronics. 2013: pp. 1384–1389.
13. Zhong QC, Zeng Y, Ren B. UDE-Based Robust Droop Control of Inverters in Parallel Operation. IEEE Transactions on Industrial Electronics. 2017;64(9):7552–7562.
14. Zhong QC. Robust Droop Controller for Accurate Proportional Load Sharing Among Inverters Operated in Parallel. IEEE Transactions on Industrial Electronics. 2013;60(4):1281–1290.
15. Zhong QC, Zeng Y. Control of Inverters Via a Virtual Capacitor to Achieve Capacitive Output Impedance. IEEE Transactions on Power Electronics. 2013;29(10):5568–5578.
16. Zhong QC, Zeng Y. Universal Droop Control of Inverters With Different Types of Output Impedance. IEEE Access. 2016;4:702–712.
17. Bhambri S, Shrivastava V, Kumawat M. Single Solution for Control and Synchronization of Inverters in Microgrids. In: 9th IEEE India International Conference on Power Electronics (IICPE), Sonipat, 28–30 November, 2023.
18. Bhambri S, Shrivastava V, Kumawat M. Improvement in power sharing performance in an AC microgrid through PI controller approach under different load condition. In: IEEE 5th International Conference on Sustainable Energy and Future Electric Transportation (SEFET), Jaipur, 9–12 July, 2025.
19. Guerrero JM, Vicuna LG. de, Matas J. Castilla, M, Miret, J. Output Impedance Design of Parallel-Connected UPS Inverters With Wireless Load-Sharing Control. IEEE Transactions on Industrial Electronics. 2005;52(4):1126–1135.
20. Dheer KD, Gupta Y, Doolla S. A Self-Adjusting Droop Control Strategy to Improve Reactive Power Sharing in Islanded Microgrid. IEEE Transactions on Sustainable Energy. 2020;11(3):1624–1635.
21. Zhu Y, Fan Q, Liu B, Wang T. An Enhanced Virtual Impedance Optimization Method for Reactive Power Sharing in Microgrids, in IEEE Transactions on Power Electronics. Dec. 2018;33(12):10390–10402.doi: 10.1109/TPEL.2018.2810249.
22. Mohammed N, Lashab A, Ciobotaru M, Guerrero JM. Accurate Reactive Power Sharing Strategy for Droop-Based Islanded AC Microgrids. in IEEE Transactions on Industrial Electronics. March 2023;70(3):2696–2707. doi: 10.1109/TIE.2022.3167141.
23. Zhou, Cheng P-T. A modified Q — V droop control for accurate reactive power sharing in distributed generation microgrid. 2017 IEEE Energy Conversion Congress and Exposition (ECCE). Cincinnati, OH, USA, 2017, pp. 4099–4106, doi: 10.1109/ECCE.2017.8096713.
24. Fan B, *et al.* A Novel Droop Control Strategy of Reactive Power Sharing Based on Adaptive Virtual Impedance in Microgrids. in IEEE Transactions on Industrial Electronics. Nov. 2022;69(11):11335–11347. doi: 10.1109/TIE.2021.3123660.
25. Mahmood H, Michaelson D, Jiang J. Reactive Power Sharing in Islanded Microgrids Using Adaptive Voltage Droop Control. in IEEE Transactions on Smart Grid. Nov. 2015;6(6):3052–3060. doi: 10.1109/TSG.2015.2399232.
26. Zhu Y, Zhuo F, Wang F, Liu B, Gou R, Zhao Y. A Virtual Impedance Optimization Method for Reactive Power Sharing in Networked Microgrid. in IEEE Transactions on Power Electronics. April 2016;31(4):2890–2904. doi: 10.1109/TPEL.2015.2450360.
27. Yu K, Ai Q, Wang S, Ni J, Lv T. Analysis and Optimization of Droop Controller for Microgrid System Based on Small-Signal Dynamic Model. IEEE Transactions on Smart Grid. 2016;7(2):695–705.
28. Rasheduzzaman M, Mueller JA, Kimball JW. An Accurate Small-Signal Model of Inverter-Dominated Islanded Microgrids Using dq Reference Frame. IEEE Journal of Emerging and Selected Topics in Power Electronics. 2014;2(4):1070–1080.
29. Pournazarian B, Seyedalipour SS, Lehtonen M, Taheri S, Pouresmaeil E. Virtual Impedances Optimization to Enhance Microgrid Small-Signal Stability and Reactive Power Sharing. IEEE Access. 2020;8:139691–139705.

30. Pournazarian B, Sangrody, Lehtonen M, Gharehpetian GB, Pouresmaeil E. Simultaneous Optimization of Virtual Synchronous Generators Parameters and Virtual Impedances in Islanded Microgrids. IEEE Transactions on Smart Grid. 2022;13(6):4202–4217.
31. Pogaku N, Prodanovic M, Green T. Modeling, Analysis and testing of autonomous operation of an inverter-based microgrid. IEEE Transactions on Power Electronics. 2007;22(2):613–625.

Appendix A

$$B_{INVi} = \begin{bmatrix} 0 & \cdots\cdots & 0 & \frac{-cos\delta}{L_c} & \frac{-sin\delta}{L_c} \\ 0 & \cdots\cdots & 0 & \frac{\sin\delta}{L_c} & \frac{-cos\delta}{L_c} \end{bmatrix}^T_{2\times 13}, \qquad B_{i\omega com} = [-1\ 0\ 0 \ldots\ldots 0]^T_{1\times 13}$$

$$C_{INV\omega i} = [0 - m\ 0 \ldots 0]_{1\times 13}\ i = 1$$
$$= [0 \ldots\ldots\ldots 0]_{1\times 13}\ i \neq 1$$

$$C_{INVci} = \begin{bmatrix} -I_{od}\ sin\delta\ -I_{oq}\ cos\delta\ ..0 \ldots 0 \ldots\ldots 0\ cos\delta, -sin\delta \\ I_{od}\ cos\delta\ -I_{oq}\ sin\delta\ ..0 \ldots . 0 \ldots\ldots 0\ sin\delta, \quad \cos\delta \end{bmatrix}_{2\times 13}$$